CRYSTAL GROWTH & DESIGN

Article

pubs.acs.org/crystal

# Heteroepitaxial Growth of Perovskite $CaTaO_2N$ Thin Films by Nitrogen Plasma-Assisted Pulsed Laser Deposition

*Published as part of the Crystal Growth & Design virtual special issue on Anion-Controlled New Inorganic Materials*

Daichi Oka,[†] Yasushi Hirose,*[,†,‡,§] Tomoteru Fukumura,[†,‡,§] and Tetsuya Hasegawa[†,‡,§]

[†]Department of Chemistry, School of Science, The University of Tokyo, 7-3-1 Hongo, Bunkyo, Tokyo 113-0033 Japan

[‡]Kanagawa Academy of Science and Technology (KAST), 3-2-1 Sakado, Takatsu, Kawasaki 213-0012 Japan

[§]CREST, Japan Science and Technology Agency, 7-3-1 Hongo, Bunkyo, Tokyo 113-0033 Japan

**ABSTRACT:** We demonstrated heteroepitaxial growth of perovskite $CaTaO_2N$ on $SrTiO_3$ (100) substrates by using nitrogen plasma assisted pulsed laser deposition (NPA-PLD). The $CaTaO_2N$ films grew coherently on $SrTiO_3$ substrates, showing a layer-by-layer growth mode in the initial stages. The obtained films possessed high crystallinity, a sharp film/substrate interface, and flat surfaces. Impedance measurements revealed that $CaTaO_2N$ has a much smaller dielectric constant than those of $SrTaO_2N$ or $BaTaO_2N$. These results indicate that heteroepitaxial growth by NPA-PLD is a promising approach for preparing high-quality perovskite oxynitride single crystals, which are desirable for investigation of electrical properties of perovskite oxynitrides.

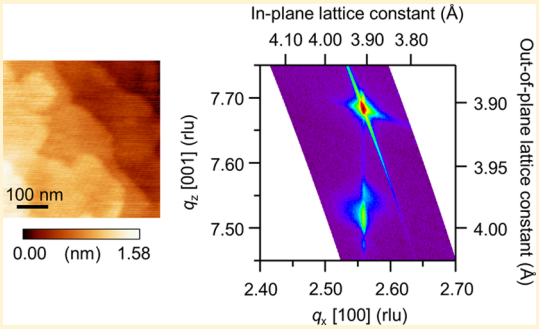


## INTRODUCTION

Perovskite oxynitrides have attracted interest for use as pigments[1] and photocatalysts[2] because of their unique band structures with narrow bandgaps. Recently, a new aspect of perovskite oxynitrides has been exploited: electrical materials with novel functionalities, such as high dielectric constants in $ATaO_2N$ (A = Sr or Ba)[4] and colossal magnetoresistance in $EuWO_{1+x}N_{2-x}$.[5]

Bulk oxynitrides are generally synthesized in fine-powder form by nitridation of oxide precursors with high-temperature ammonia.[4,6] Thermal decomposition of oxynitrides makes it difficult to obtain dense ceramics or single crystals from the powders, preventing reliable measurement of their electrical properties. Although topotactical nitridation of $A_2B_2O_7$-type layered perovskite oxides is a practical way to synthesize perovskite oxynitrides in a single-crystalline thin-layer form,[7] unreacted parts of the precursor oxide crystals sometimes hinder electrical measurements. Therefore, it is still important to establish a feasible route to synthesize high-quality oxynitride crystals.

Epitaxial growth of thin films on lattice-matched substrates is a promising approach to obtain single-crystalline samples. In the case of perovskite oxides, indeed, epitaxial thin films have been widely used to study their electrical properties. On the other hand, the quality of perovskite oxynitride epitaxial thin films, as fabricated by sputtering or pulsed laser deposition,[8−11] is generally inferior to that of perovskite oxide thin films. This is partly because of the difficulty in controlling anion composition, since nitrogen is easily released from the films at high temperature.

Recently, we succeeded in epitaxial growth of stoichiometric $SrTaO_2N$[12] thin films using the nitrogen plasma assisted pulsed laser deposition (NPA-PLD) method, in which the balance between supplies of nitrogen and the other elements is precisely controllable. The obtained films showed high crystallinity and low enough leakage currents to be suitable for dielectric measurements. However, the films were partially relaxed from the $SrTiO_3$ (STO) substrates, and their surfaces were not atomically flat (root-mean-square (RMS) roughness of 2.0 nm). The lattice relaxation and surface roughness may be because of the large lattice mismatch between film and substrate (−3.1%), which can result in three-dimensional growth.

In this study, we report heteroepitaxial NPA-PLD growth of $CaTaO_2N$, which in a pseudocubic approximation has better lattice matching with STO (−1.1%). We found that $CaTaO_2N$ can be coherently grown on STO. The obtained $CaTaO_2N$ films showed high crystallinity, atomically flat surface, and sharp film/substrate interface, as well as low leakage current, which ensured reliable electrical measurements. The dielectric constant of the $CaTaO_2N$ films was much smaller than those of bulk $SrTaO_2N$ and $BaTaO_2N$, as suggested in previous measurements on a bulk sample.[4]

**Received:** August 2, 2013
**Revised:** November 26, 2013
**Published:** December 11, 2013

  

## EXPERIMENTAL SECTION

$CaTaO_2N$ ($a$ = 3.9477 Å under pseudocubic approximation[4]) epitaxial thin films were grown on (100) planes of pure STO and 0.5 wt % Nb-doped STO ($a$ = 3.905 Å) substrates with atomically flat surface (Shinkosha Co., Ltd.) by the NPA-PLD method. A $Ca_2Ta_2O_7$ ceramic pellet was used as a target, which was obtained by sintering $Ca_2Ta_2O_7$ powder at 1400 °C for 50 h. The $Ca_2Ta_2O_7$ powder was synthesized by conventional solid phase reaction of a stoichiometric mixture of $Ta_2O_5$ and $CaCO_3$ in an alumina crucible: The reaction was first conducted at 800 °C for 24 h and successively heated at 1000 °C for 24 h, and 1200 °C for 50 h. The substrate temperature and partial pressure of $N_2$ gas ($P_{N2}$) were set at 800 °C and $1.0 \times 10^{-5}$ Torr, respectively. $N_2$ gas was activated into radicals by a radio frequency (RF) plasma source (SVT Associates, model 4.5") with input power of 250 W. The plasma source was equipped with a parallel plate capacitor (ion deflector) to remove ionic species from the plasma. A KrF excimer laser ($\lambda$ = 248 nm) operated at an energy density of 0.4 J $cm^{-1}$ $shot^{-1}$, and a repetition rate of 20 Hz was used for ablation. Thickness of the films prepared in this study was within the range of 19 to 37 nm, and typical deposition rate was 10−20 nm/h, at which the oxygen supplied from the target and nitrogen from the plasma source were balanced. The growth mode of the thin films was monitored in situ by reflection high energy electron diffraction (RHEED).

Surface morphology of the thin films was characterized with an atomic force microscope (AFM) (SII-nanotechnology, SPI4000 with SPA400). The nitrogen content $y$ in $CaTaO_xN_y$ was determined by nuclear reaction analysis (NRA) using the $^{15}N(p,\alpha\gamma)^{12}C$ reaction. Because we used natural $N_2$ gas ($^{15}N/^{14}N$ = ∼0.37%) as a nitrogen source, the concentrations of $^{15}N$ in the samples were low ($10^{17}$ $cm^{-2}$ order). Therefore, energy of incident proton beam was set at 898 keV resonance of the reaction to enhance the reaction cross section. The NRA measurements were carried out with a 1 MV tandetron accelerator at Tandem Accelerator Complex, University of Tsukuba. Two 3-in. $Bi_4Ge_3O_{12}$ scintillation counters were used to detect the emitted $\gamma$-ray. A TiN thin film was used as a reference sample for nitrogen. The oxygen content $x$ was calculated from $y$ by assuming charge neutrality and a Ca/Ta ratio of unity. Crystal structures of the thin films were evaluated by X-ray diffraction (XRD) using a four-axis diffractometer (Bruker AXS, d8 discover). Microscopic structures were also investigated by cross-sectional transmission electron microscopy (TEM) (Hitachi, H-9000NAR, 300 kV). Optical band gap values of the thin films were evaluated based on absorption spectrum calculated from optical extinction coefficients determined by a spectroscopic ellipsometer (J.A. Woollam, M-2000U). Impedance measurements were conducted in the capacitor configuration of Pt/$CaTaO_2N$/0.5 wt % Nb-doped STO using a precision LCR-meter (Agilent, E4980A) over a frequency range of 1 kHz to 100 kHz. Dielectric constant, $\varepsilon'$, and tangent loss, tan $\delta$, of the film were calculated assuming a simple parallel circuit composed of a resistor and a capacitor. Pt top electrodes (200 $\mu m\varphi$) were sputtered onto the $CaTaO_2N$ thin films. To suppress leakage current, the as-grown $CaTaO_2N$ thin films were further annealed at 500 °C for 30 h under a mixture of nitrogen ($P_{N2}$ = $1.0 \times 10^{-5}$ Torr, activated by RF plasma source) and oxygen (partial pressure of $2.0 \times 10^{-5}$ Torr) gas before the measurements.

## RESULTS AND DISCUSSION

Figure 1a shows RHEED intensity oscillation during the deposition. Clear oscillation continued for at least 15 cycles, indicating layer-by-layer growth of the epitaxial $CaTaO_2N$ thin films. The streak-shaped diffraction pattern was still observed after the deposition (Figure 1b), assuring good crystallinity and flat surface of the films.

As shown in the AFM images (Figure 2a,b), the surface of the $CaTaO_2N$ thin films was indeed atomically flat with a step-and-terrace structure, though small islands were recognizable in the wide-scan image. The RMS roughness evaluated from Figure 2a was 0.14 nm, which is much less than that of the $SrTaO_2N$ thin film (2.0 nm). The step height calculated from

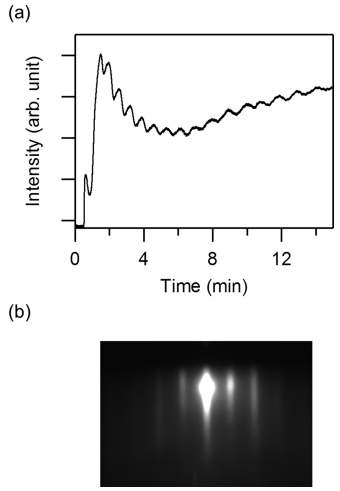


**Figure 1.** (a) RHEED intensity oscillation during the deposition of $CaTaO_2N$ thin film on STO substrate. (b) RHEED pattern of $CaTaO_2N$ thin film on STO substrate after deposition.

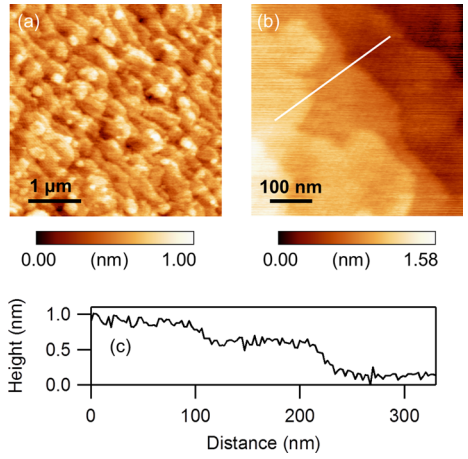


**Figure 2.** (a, b) AFM images of $CaTaO_2N$ epitaxial thin film on Nb-doped STO substrate at different length scales. (c) Line profile along the white line in (b).

the cross-section (Figure 2c) was ∼0.4 nm, corresponding very well to the length of a $CaTaO_2N$ pseudocubic unit cell.

As far as we know, this is the first report of layer-by-layer growth of a perovskite oxynitride thin film with atomically flat surface. The chemical composition of the $CaTaO_2N$ thin films was determined as $CaTaO_{1.94(11)}N_{1.04(7)}$, which is essentially stoichiometric within experimental error.

Figure 3a shows the typical $\theta$−$2\theta$ profile of a $CaTaO_2N$ film grown on a Nb-doped STO (001) substrate. Only the 00$h$ diffractions of perovskite $CaTaO_2N$ were observed, with no impurity peaks. Asymmetric reflection measurements of $h0h$ diffractions also confirmed the growth of phase-pure perovskite $CaTaO_2N$ (data not shown). The fringe pattern around the 001 diffraction in the high-resolution $\theta$−$2\theta$ profile (inset of Figure 3a) reveals a sharp interface between the films and substrates. The full width at half-maximum value of the rocking curve of the 001 diffraction was 0.02°, which demonstrates the high crystallinity of the films. In order to investigate the epitaxial strain on the $CaTaO_2N$ films in more detail, an XRD reciprocal space map (RSM), which records diffraction intensity distribution of a specific diffraction in the reciprocal space, was measured around the 103 diffraction. The obtained RSM


dx.doi.org/10.1021/cg401176j | Cryst. Growth Des. 2014, 14, 87−90

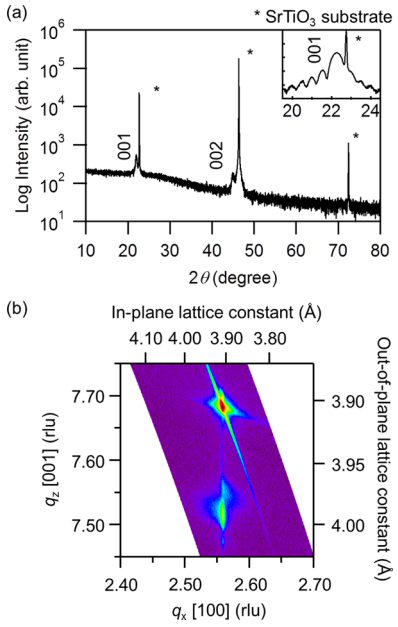


**Figure 3.** (a) XRD $\theta$–$2\theta$ profile of $CaTaO_2N$ epitaxial thin film on Nb-doped STO substrate. Inset shows the fringe pattern around the 001 diffraction. (b) XRD RSM around the 103 diffractions of $CaTaO_2N$ epitaxial thin film and Nb-doped STO substrate.

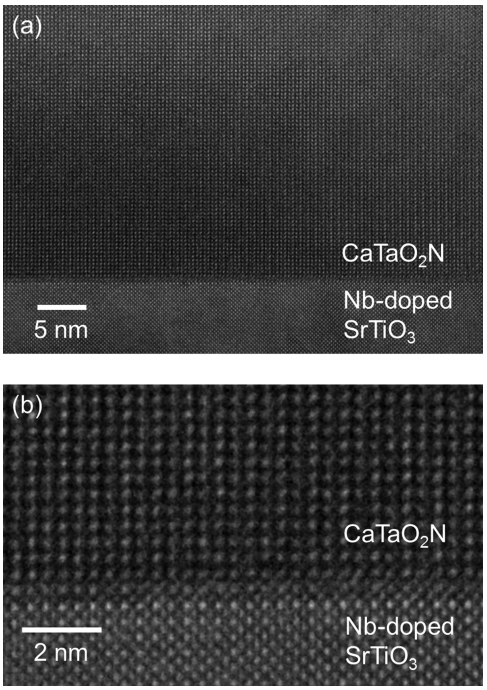


**Figure 4.** (a) Cross-sectional TEM image of $CaTaO_2N$ epitaxial thin film on Nb-doped STO substrate. (b) Magnified image of the film/substrate interface.

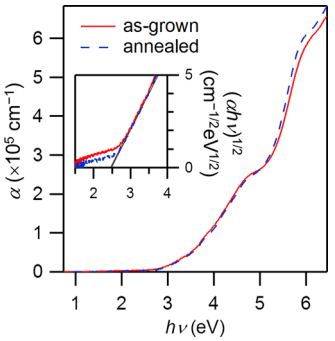


**Figure 5.** Spectral absorption coefficients of $CaTaO_2N$ epitaxial thin films on STO substrate calculated from optical extinction coefficients measured by spectroscopic ellipsometry. Solid line (red) and dashed line (blue) are the spectra before and after the post-deposition annealing. Inset shows the $(\alpha\ h\nu)^{1/2}$ vs $h\nu$ plots to determine the optical band gaps. Black lines in the inset are the results of linear fitting for the higher $h\nu$ regions.

(Figure 3b) shows tetragonal distortion of the $CaTaO_2N$ films caused by the compressive strain from the STO substrate. The lattice parameters of the $CaTaO_2N$ films, evaluated from the RSM, were $a$ = 3.905 Å and $c$ = 3.99 Å. Note that the in-plane lattice constant was perfectly locked to the STO substrate; that is, the $CaTaO_2N$ films were coherently grown on STO. The $c$-axis length is much longer than the values deduced from lattice constants of bulk $CaTaO_2N$ ($a/\sqrt{2}$ = 3.97320 Å, $b/2$ = 3.94655 Å, $c/\sqrt{2}$ = 3.92358 Å[4]), which also validates the epitaxial stress from the substrates.

This is in sharp contrast to the $SrTaO_2N$ epitaxial thin films ($a$ = 4.03 Å under a pseudocubic approximation,[13] −3.1% mismatch), which was partially relaxed from the STO substrate.[12] Similar lattice relaxation was also reported in $BaTaO_2N$ epitaxial thin films ($a$ = 4.113 Å[14]) grown on $SrRuO_3$-buffered STO substrate ($a$ = 3.95 Å under a pseudo cubic approximation,[14] −4.1% mismatch).[14] Thus, the coherent growth and resultant flat surface and high crystallinity appear to be related to the smaller lattice mismatch between $CaTaO_2N$ and STO. We did not find any significant difference in surface morphology and crystal structure between the films grown on STO and Nb-doped STO.

The crystal growth manner and microscopic structure of the $CaTaO_2N$ thin films were cross-checked with cross-sectional TEM observations. The obtained TEM images (Figure 4a,b) clearly exhibit sharp film/substrate interface and coherent growth of the $CaTaO_2N$ films without segregation of any secondary phases.

Optical properties of the $CaTaO_2N$ thin films were investigated by spectroscopic ellipsometry. Figure 5 shows absorption spectra of the as-grown and annealed $CaTaO_2N$ thin films, where the absorption coefficient $\alpha$ was calculated from the optical extinction coefficient $k$ ($\alpha = 4\pi k\lambda^{-1}$). Although the detailed band structure of $CaTaO_2N$ has not been reported so far, good linear relations of the $(\alpha\ h\nu)^{1/2}$ vs $h\nu$ plots suggest that the absorption mechanism of our thin films is indirect transition (inset of Figure 5). The band gap was determined as ∼2.5 eV, which is in good agreement with the reported value of bulk specimen (2.4 eV).[4] Notably, the band gap value did not change at all after the annealing process to suppress leakage current, which ensures the nitrogen content was conserved.

Finally, we briefly mention the dielectric properties of the $CaTaO_2N$ thin films. In the previous study on bulk perovskite oxynitrides, it was suggested that the $\varepsilon'$ value of $CaTaO_2N$ ($\varepsilon' \approx 30$) is much smaller than those of $SrTaO_2N$ or $BaTaO_2N$ ($\varepsilon' > 2000$). However, the small dielectric constant of $CaTaO_2N$ was not a very conclusive result, because it was difficult to separate the bulk and grain boundary components of $\varepsilon'$ in the impedance measurements.[4] To examine the $\varepsilon'$ of $CaTaO_2N$, we performed impedance measurements of the $CaTaO_2N$ epitaxial thin films, in which the contribution of grain boundaries should


dx.doi.org/10.1021/cg401176j | Cryst. Growth Des. 2014, 14, 87−90

be negligible. The observed tangent loss, tan $\delta$ < 0.01, is rather low compared with the previously reported values for perovskite oxynitrides[4,6,9,12,15,16] (Figure 6a). Furthermore,

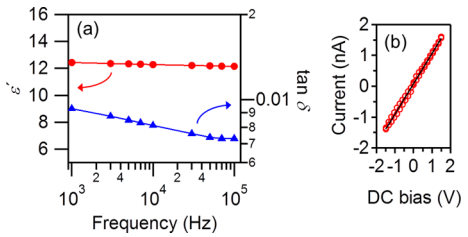


**Figure 6.** (a) Frequency dependence of dielectric constant ($\varepsilon'$) (red circle) and tan $\delta$ (blue triangle) of the annealed $CaTaO_2N$ epitaxial thin film on Nb-doped STO substrate. (b) $I-V$ curve of the annealed $CaTaO_2N$ epitaxial thin film on Nb-doped STO substrate. A solid line is the result of linear fitting.

the DC resistance value evaluated from the $I-V$ curve (Figure 6b) is as high as ~1 GΩ. Such highly insulating properties are probably the consequence of excellent crystallinity as well as considerable suppression of oxygen vacancies by the post-deposition annealing. Dielectric constant $\varepsilon'$ of the $CaTaO_2N$ thin film was approximately 12, almost independent of frequency between 1 kHz and 100 kHz (Figure 6a). This value is comparable to that of bulk $CaTaO_2N$ ($\varepsilon' \approx 30$),[4] suggesting that the small $\varepsilon'$ is intrinsic to $CaTaO_2N$.

## CONCLUSIONS

We succeeded in heteroepitaxial growth of stoichiometric $CaTaO_2N$ thin films on STO substrates by a NPA-PLD method. We confirmed that $CaTaO_2N$ grows as a coherent high-crystallinity single crystal with a sharp film/substrate interface and atomically flat surface. These features have not previously been achieved in epitaxial growth of perovskite oxynitrides. The dielectric loss was as low as <0.01, also implying relatively low defect density. The dielectric constant of the $CaTaO_2N$ films was comparable to that of the bulk sample, validating the previous suggestion that the low dielectric constant is an intrinsic property of $CaTaO_2N$. NPA-PLD has been shown to be a powerful tool for heteroepitaxial growth of oxynitride thin films. The high-quality thin films obtained by this method will allow us to study intrinsic electrical properties of oxynitrides, which includes not only dielectric properties in insulating samples but also carrier transports in conducting ones.

## AUTHOR INFORMATION

### Corresponding Author

*E-mail: hirose@chem.s.u-tokyo.ac.jp. Tel: +81-44-819-2081. Fax: +81-44-819-2083.

### Funding

This study was supported by the Ministry of Education, Culture, Sports, Science and Technology (MEXT), Japan, as part of KAKENHI No. 24760005 and Japan Society for the Promotion of Science (JSPS) KAKENHI Grant Number No. 248258. A part of this work was conducted in Research Hub for Advanced Nano Characterization, The University of Tokyo, under the support of "Nanotechnology Platform" by MEXT, Japan.

### Notes

The authors declare no competing financial interest.

## ACKNOWLEDGMENTS

We thank Mr. Seiji Ito, Mr. Akira Morita, Prof. Hiroyuki Matsuzaki, and Prof. Katsuyuki Fukutani of the University of Tokyo and Prof. Kimikazu Sasa, Dr. Daiichiro Sekiba, Dr. Hiroshi Naramoto, and Mr. Satoshi Ishii of University of Tsukuba for their assistance with the NRA measurements.

## ABBREVIATIONS

NPA-PLD, nitrogen plasma assisted pulsed laser deposition; STO, $SrTiO_3$; RMS, root-mean-square; RF, radio frequency; AFM, atomic force microscope; NRA, nuclear reaction analysis; XRD, X-ray diffraction; TEM, transmission electron microscopy; RSM, reciprocal space map

## REFERENCES

(1) Fuertes, A. *Dalton Trans.* **2010**, *39*, 5942−5948.
(2) Jansen, M.; Letschert, H. *Nature* **2000**, *404*, 980−982.
(3) Kasahara, A.; Nukumizu, K.; Hitoki, G.; Takata, T.; Kondo, J. N.; Hara, M.; Kobayashi, H.; Domen, K. *J. Phys. Chem. A* **2002**, *106*, 6750−6753.
(4) Kim, Y.-I.; Woodward, P. M.; Baba-Kishi, K. Z.; Tai, C. W. *Chem. Mater.* **2004**, *16*, 1267−1276.
(5) Yang, M.; Oró-Solé, J.; Kusmartseva, A.; Fuertes, A.; Attfield, J. P. *J. Am. Chem. Soc.* **2010**, *132*, 4822−4829.
(6) Zhang, Y.-R.; Motohashi, T.; Masubuchi, Y.; Kikkawa, S. *J. Eur. Ceram. Soc.* **2012**, *32*, 1269−1274.
(7) Ebbinghaus, S. G.; Aguiar, R.; Weidenkaff, A.; Gsell, S.; Reller, A. *Solid State Sci.* **2008**, *10*, 709−716.
(8) Lekshmi, I. C.; Gayen, A.; Hegde, M. S. *Mater. Res. Bull.* **2005**, *40*, 93−104.
(9) Kim, Y.-I.; Si, W.; Woodward, P. M.; Sutter, E.; Park, S.; Vogt, T. *Chem. Mater.* **2007**, *19*, 618−623.
(10) Aguiar, R.; Logvinovich, D.; Weidenkaff, A.; Karl, H.; Schneider, C.; Reller, A.; Ebbinghaus, S. *Mater. Res. Bull.* **2008**, *43*, 1376−1383.
(11) Le Paven-Thivet, C.; Ishikawa, A.; Ziani, A.; Le Gendre, L.; Yoshida, M.; Kubota, J.; Tessier, F.; Domen, K. *J. Phys. Chem. C* **2009**, *113*, 6156−6162.
(12) Oka, D.; Hirose, Y.; Kamisaka, H.; Fukumura, T.; Sasa, K.; Ishii, S.; Matsuzaki, H.; Sato, Y.; Ikuhara, Y.; Hasegawa, T. submitted for publication, 2013.
(13) Marchand, R.; Pors, F.; Laurent, Y.; Regreny, O.; Lostec, J.; Haussonne, J. M. *J. Phys. Colloques* **1986**, *47*, C1−901−C1−905.
(14) Kim, Y.-I.; Si, W.; Woodward, P. M.; Sutter, E.; Park, S.; Vogt, T. *Chem. Mater.* **2007**, *19*, 618−623.
(15) Zhang, Y.-R.; Masubuchi, Y.; Motohashi, T.; Kikkawa, S.; Hirota, K. *Ceram. Int.* **2013**, *39*, 3377−3380.
(16) Ziani, A.; Le Paven-Thivet, C.; Le Gendre, L.; Fasquelle, D.; Carru, J.; Tessier, F.; Pinel, J. *Thin Solid Films* **2008**, *517*, 544−549.